ACS APPLIED MATERIALS & INTERFACES

Research Article

www.acsami.org

Hydration and Chain Entanglement Determines the Optimum Thickness of Poly(HEMA-*co*-PEG$_{10}$MA) Brushes for Effective Resistance to Settlement and Adhesion of Marine Fouling Organisms

Wetra Yandi,[†] Sophie Mieszkin,[‡] Pierre Martin-Tanchereau,[§,∥] Maureen E. Callow,[‡] James A. Callow,[‡] Lyndsey Tyson,[§] Bo Liedberg,[†] and Thomas Ederth*[,†]

[†]Division of Molecular Physics, IFM, Linköping University, 581 83 Linköping, Sweden

[‡]School of Bioscience, University of Birmingham, Birmingham B15 2TT, United Kingdom

[§]International Paint Ltd, Gateshead NE10 0JY, United Kingdom

[∥]Department of Applied Sciences, Northumbria University, Newcastle upon Tyne NE1 8ST, United Kingdom

Supporting Information

ABSTRACT: Understanding how surface physicochemical properties influence the settlement and adhesion of marine fouling organisms is important for the development of effective and environmentally benign marine antifouling coatings. We demonstrate that the thickness of random poly(HEMA-*co*-PEG$_{10}$MA) copolymer brushes affect antifouling behavior. Films of thicknesses ranging from 50 to 1000 Å were prepared via surface-initiated atom-transfer radical polymerization and characterized using infrared spectroscopy, ellipsometry, atomic force microscopy and contact angle measurements. The fouling resistance of these films was investigated by protein adsorption, attachment of the marine bacterium *Cobetia marina*, settlement and strength of attachment tests of zoospores of the marine alga *Ulva linza* and static immersion field tests. These assays show that the polymer film thickness influenced the antifouling performance, in that there is an optimum thickness range, 200−400 Å (dry thickness), where fouling of all types, as well as algal spore adhesion, was lower. Field test results also showed lower fouling within the same thickness range after 2 weeks of immersion. Studies by quartz crystal microbalance with dissipation and underwater captive bubble contact angle measurements show a strong correlation between lower fouling and higher hydration, viscosity and surface energy of the poly(HEMA-*co*-PEG$_{10}$MA) brushes at thicknesses around 200−400 Å. We hypothesize that the reduced antifouling performance is caused by a lower hydration capacity of the polymer for thinner films, and that entanglement and crowding in the film reduces the conformational freedom, hydration capacity and fouling resistance for thicker films.

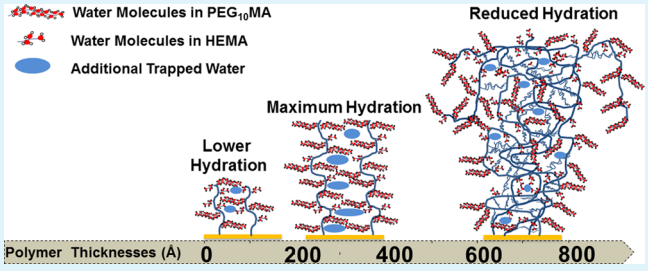

KEYWORDS: *marine fouling, polymer brushes, SI-ATRP, fibrinogen, Cobetia marina, Ulva linza*

INTRODUCTION

Marine biofouling is unwanted accumulation of marine microorganisms, plants, algae, or animals on surfaces submerged in natural waters.[1] This is a worldwide phenomenon and a major problem in marine industries due to its great economic and environmental impact. The speed of ships is significantly reduced by the presence of marine biofouling. It has been estimated that heavy calcareous biofouling on a ship hull could increase the required shaft power by 86%, as compared to an equivalent vessel with a smooth hull.[2] This power loss leads to increased fuel consumption, resulting in higher emissions of CO_x, SO_x and NO_x, which contributes to the destruction of the ozone layer, enhanced greenhouse effect and acid rain.[3] In addition, marine biofouling is a significant problem in other marine-related industries, as fouling organisms also colonize and corrode immersed man-made surfaces on oceanographic instrumentation, power plant water intakes, heat exchangers and condensers, membrane bioreactors, aquaculture equipment and water desalination systems.[4] The development of technologies to combat marine biofouling has taken place over 2000 years. Antifouling paints containing copper and toxic biocides have been considered as successful technologies over the last few decades, because they are broadly efficient against many fouling species.[5] However, the use of copper and certain biocides has been restricted through legislation due to environmental concerns.[6] Recently, development of environmentally benign antifouling coatings has become an attractive and challenging issue in marine biofouling research.[7]

Received: April 6, 2014
Accepted: June 19, 2014
Published: June 19, 2014

Understanding how physicochemical properties of surfaces influence the attachment, adhesion and settlement of fouling organisms is essential for the development of new nontoxic antifouling technologies and in designing effective and environmentally benign antifouling coatings. To this end, fouling on well-defined and carefully characterized surface chemistries, such as various oligoethylene glycol self-assembled monolayers (OEG SAMs),[8,9] peptide SAMs,[10,11] saccharide SAMs[12,13] and polymers[14−16] and physicochemical properties such as wettability,[9,17] surface energy,[18,19] roughness,[20,21] thickness[22] elastic modulus[22,23] charge[18,24] and several other properties[25] have been studied intensively to understand the role of surface properties on the mechanisms responsible for settlement and adhesion of fouling organisms.

In recent years, antifouling coatings based on hydrophilic polymers have received growing attention due to their promising potential as environmentally benign marine antifouling coatings.[14,26] Some properties of hydrophilic materials, such as softness and strong hydration are considered important for effective antifouling or low adhesion by fouling species. With regard to how the antifouling properties depend of coating thickness, this has been studied for protein adsorption in a number of systems, including early and fundamental work on poly(ethylene glycol) (PEG) coatings,[27,28] and more recent work on both hydrophilic and zwitterionic polymers.[29,30] With regard to marine fouling, in particular, there appears to be few studies on how polymer layer thicknesses influence fouling behavior, apart from the well-documented studies on the influence of polymer (PDMS) thickness at the scale of tens to hundreds of micrometres on the adhesion strength of macrofouling.[22,31]

In this work, a series of random poly(HEMA-*co*-$PEG_{10}MA$) copolymer films with thicknesses from 50 to 1000 Å have been prepared via surface-initiated atom transfer radical polymerization (SI-ATRP), and the influence of polymer thickness on antifouling performance against some marine fouling species was studied in detail. We also discuss how surface physicochemical properties such as surface hydration, polymer viscoelasticity and surface energy are influenced by variations in the polymer thickness.

The HEMA-*co*-$PEG_{10}MA$ random copolymer was selected in this study for several reasons. PEG brushes have excellent antifouling properties, but are also subject to chemical degradation, and are thus unsuitable for many practical applications. A popular strategy for finding alternative materials with the antifouling properties of PEG, but with better stability, is to attach PEG side-chains to a more stable backbone, and we use PEG-based polymers graft copolymerized onto substrates from PEG methacrylate mixtures for this purpose, and have shown that these polymers are suitable for biochip and biosensor applications in demanding biofluids, and also resistant to marine fouling organisms.[14,32] From previous work, we have observed that HEMA-$PEG_{10}MA$ copolymers form layers with better antifouling properties and stability than homopolymers of either component.[14,32] Further, previous work[33] on $PEG_{10}MA$ polymers indicates a faster decrease in growth rate than we obtain with poly(HEMA-*co*-$PEG_{10}MA$), and it thus seems easier to reach large film thicknesses using the copolymer blend. Finally, compared to the homopolymers of either HEMA or $PEG_{10}MA$, the copolymer is significantly easier to polymerize using self-initiated photografting and photopolymerization, a method that we have used in several previous studies,[14,32] and comparison of results across preparation methods with the same polymer composition will facilitate understanding of the antifouling properties of these coatings.

MATERIALS AND METHODS

Materials. 2-Hydroxyethyl methacrylate (HEMA), polyethylene glycol methacrylate ($PEG_{10}MA$), copper(I) bromide (99.999%), 2,2-bipyridine (BPY, 99%) and fibrinogen were purchased from Sigma-Aldrich Sweden AB. α-Bromoisobutyrate-11-mercaptoundecane (ProChimia, Poland) was used to form initiator-layer SAMs. Hexadecanethiol was obtained from Fluka. All biological evaluation experiments were carried out using glass microscope slides (cleanroom-cleaned Nexterion B, 26 × 76 × 1 mm, Schott AG, Germany) coated on one side with polymer. Phosphate-buffered saline (PBS) was prepared by dissolving PBS tablets (Sigma-Aldrich Sweden AB) into 200 mL of Milli-Q water) and adjusting to pH 7.4.

Preparation of Initiator Layers. Glass substrates were coated with titanium (25 Å, adhesion-promoting layer) and gold (300 Å) by electron-beam evaporation under a vacuum. Before immobilization of the initiator, the gold-coated glass substrates were cleaned in TL1 solution (1:1:5 proportions of 25% NH_3, 30% H_2O_2 and Milli-Q water for 10 min at 85 °C) washed with Milli-Q water several times and dried in a N_2 stream. Cleaned gold substrates were then immersed in 50 μM of α-bromoisobutyrate-11-mercaptoundecane in ethanol solution for 24 h to form the initiator layer for SI-ATRP. Before use, the SAM-coated gold substrates were rinsed in sequence with ethanol and water and then dried in a N_2 stream. Methyl-terminated hexadecanethiol SAMs (henceforth referred to as CH_3 SAMs) were prepared from 50 μM solutions in ethanol, as above.

Preparation of Poly(HEMA-*co*-$PEG_{10}MA$) Films. Different thicknesses of random copolymer poly(HEMA-*co*-$PEG_{10}MA$) brushes were prepared via the surface-initiated atom transfer radical polymerization (SI-ATRP) method (shown in Figure 1), which has been

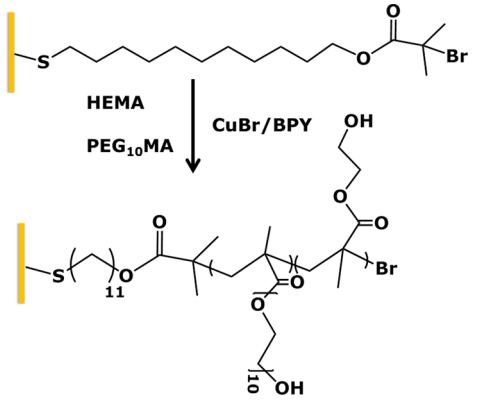

Figure 1. Preparation of poly(HEMA-*co*-$PEG_{10}MA$) onto an initiator-immobilized gold surface (top) via surface-initiated atom transfer radical polymerization (SI-ATRP).

reported previously.[34−36] Briefly, the reaction solution of 2.41 mM copper bromide and 4.68 mM 2,2′-bipyridine was placed in a sealed glass reactor in a glovebox under a N_2 atmosphere. Then, 200 mM degassed HEMA and $PEG_{10}MA$ (molar ratio 1:1) solution in a mixing solvent (Milli-Q water and methanol at a 1:1 volume ratio) was transferred to the reactor. Gold surfaces with immobilized initiator-SAMs were then placed into the reactor under N_2 protection at room temperature (20 °C) (Figure 1). To obtain the different thicknesses, various SI-ATRP polymerization times were used. After polymerization, samples were removed and rinsed with water and methanol and the samples were kept in water overnight to leach out chemical residues and unbound monomers.

Polymer Characterization. The chemical structure of poly(HEMA-*co*-$PEG_{10}MA$) was characterized by Fourier-transform infrared reflection−absorption spectroscopy (FT-IRAS) using a grazing

angle of 85°. The spectrometer (Bruker IFS66) was equipped with a liquid nitrogen-cooled mercury cadmium telluride detector. A deuterated hexadecanethiol ($HS(CD_2)_{15}CD_3$) SAM on gold was used to record the background spectrum. Polymer film thicknesses of poly(HEMA-*co*-PEG_{10}MA) were determined by ellipsometric measurement using a Rudolph Research AutoEL with a HeNe laser (632.8 nm) at an angle of incidence of 70°. The refractive indices of the cleaned gold substrates were measured prior to sample preparation. A three-layer optical model (ambient/organic film/gold) was used to determine polymer film thickness, assuming an isotropic, transparent organic layer with a refractive index of n = 1.5. The polymer film thickness was calculated as an average of measurements at five different spots for each sample for each compound. To evaluate the surface wettability of poly(HEMA-*co*-PEG_{10}MA) coatings, static and dynamic (advancing and receding) water contact angles were measured using a CAM 200 optical contact angle meter (KSV Instruments Ltd., Finland) equipped with a manual liquid dispenser. Three points of the water droplet were measured on each surface. Advancing and receding contact angles were measured upon expanding and reducing the volume of the water droplet. A NanoScope IVa Dimension 3100 SPM (Veeco Instruments, Inc., USA) atomic force microscopy (AFM) instrument was used to determine the surface topography of poly(HEMA-*co*-PEG_{10}MA) at four different thicknesses (50, 200, 600 and 1000 Å). The data were acquired in tapping mode in air over an area 5 × 5 μm with a scan rate of 1 Hz.

Polymer Stability Test. To evaluate the stability of polymer brushes in seawater, six different thicknesses (50, 100, 200, 400, 600 and 1000 Å) of poly(HEMA-*co*-PEG_{10}MA) were incubated in artificial seawater (ASW) for 1 week and 3 months, respectively; this was done at 5 °C to avoid the growth of bacteria. ASW was prepared by dissolving sodium chloride (24.5 g), sodium sulfate (4.1 g), magnesium chloride hexahydrate (11.1 g), calcium chloride dihydrate (1.5 g) and potassium chloride (0.7 g) in 1 L of Milli-Q water. The solution was adjusted to pH 8.2 with 0.1 M NaOH, and subsequently filtered with a 0.2 μm filter (Nalgene, USA). Prior to incubation, water contact angles and ellipsometric thicknesses of samples were measured. After 1 week or 3 months, the samples were washed several times with Milli-Q water to remove remaining salts on the surfaces and blow dried with an N_2 stream, before repeating the surface wettability and thickness measurements.

Wet Properties of Poly(HEMA-*co*-PEG_{10}MA). *Hydration and Viscoelasticity.* A Q-Sense E4 quartz crystal microbalance with dissipation (QCM-D) was used to measure the absorbed amount of water and the viscoelasticity of hydrated poly(HEMA-*co*-PEG_{10}MA). AT-cut quartz crystal sensors (Q-Sense, Göteborg, Sweden) with a fundamental resonant frequency of 4.950 MHz and a diameter of 14 mm were coated with 100, 200, 300, 400, 500, 600, 700, 800 or 900 Å of poly(HEMA-*co*-PEG_{10}MA) via SI-ATRP as described above. The quartz crystal was then mounted in the QCM-D fluid cell. The measurement was recorded at three different overtones (3rd, 5th and 7th) at 22 °C. For each sample, a N_2 stream with constant pressure was used for 10 min prior to the measurement to stabilize and dry the surface from moisture. Then, Milli-Q water at constant flow rate (0.3 mL/min) was added to the samples. The frequency changes (Δf) and dissipation changes (ΔD) in water were then recorded using the uncoated sensor as the reference. The frequency and dissipation differences measured between uncoated and polymer-coated sensors in Milli-Q water were defined as Δf_{film} and ΔD_{film}, respectively. The Δf and ΔD data were analyzed using QTools v3.1.24 software. To determine the viscosity and elasticity (shear modulus) of polymer films, the data were modeled using a one-layer viscoelastic Voigt model. Fixed parameters used in this experiment were the fluid density (1000 kg/m^3), fluid viscosity (0.001 kg/ms) and the density of the layer (1000 kg/m^3). The layer parameters to be fitted were kept within boundaries: viscosity (0.0001−0.01 kg/ms), shear (10^4−10^8 Pa), and layer thickness was adjusted for each sample by referring to dry thickness data measured by ellipsometry.

Surface Energy. The captive bubble technique was used to measure the contact angle of hydrated poly(HEMA-*co*-PEG_{10}MA) using a Dataphysics OCA35 contact angle analyzer with software SCA22. Samples were equilibrated in Milli-Q water for at least 1 h prior to measurement and were then placed with the coating facing downward in a glass cell filled with deionized water. A U-shaped needle was used to release 2 μL of air or *n*-octane bubbles to the polymer surfaces, under control of a computer system. Three contact angles were measured for air bubbles θ_a and *n*-octane θ_o, and were averaged; the angles were measured inside the bubble and oil droplet, respectively. The surface energy was calculated using the Owens and Wendt approach[37] applied to underwater contact angles.[38]

Biofouling Assays. *Protein Adsorption.* In this work, fibrinogen was used as it is a well-established model protein to investigate resistance to protein adsorption, due to its ability to adhere strongly to many different types of surface. Prior to the assay, the thickness of polymer samples was measured by ellipsometry to obtain the initial thickness. The samples were then washed three times with PBS and followed by 1 h of incubation in PBS at room temperature to let the polymer film swell. After removing the PBS, the samples were then incubated in fibrinogen solution (0.4 mg/mL in PBS) for 1 h at room temperature. After washing three times with PBS, the samples were then blow-dried gently with a N_2 stream and the thickness was remeasured to obtain the final thickness. The protein adsorbed on the sample surfaces is defined as the thickness difference before and after incubation.

Attachment of the Marine Bacterium Cobetia marina. In this assay, three replicates of four different thicknesses (100, 200, 400 and 600 Å) of poly(HEMA-*co*-PEG_{10}MA) were used. Additionally, three replicates of hydrophobic CH_3 SAMs, and hydrophilic Nexterion glass slides were used as reference coatings. The polymer sample slides were equilibrated in artificial seawater (ASW; Tropic Marin) for 1 h prior to assay. Cells of *Cobetia marina*[39,40] (strain ATCC 25374$_T$, DSMZ, Germany) were cultured and prepared for bioassay as described by Mieszkin et al.[41] The final stage of the protocol involved two washes of the cells in filtered ASW to remove excess extracellular polymeric substances that interfere with cell attachment.[42] The final bacterial suspension had an $OD_{600\ nm}$ = 0.1 (4 × 10^7 cells/mL). The slides were placed in polystyrene Quadriperm dishes (Greiner Bio-One Ltd.) and 10 mL of bacterial suspension was added to each well. Then, dishes were placed on a rotary shaker at room temperature and shaken for 1 h at 50 rpm to allow attachment of bacteria to the test surfaces. After removing the bacterial suspension, the slides were washed with 10 mL of ASW on a rotary shaker for 1 min at 50 rpm to remove any loosely bound cells. To evaluate the bacterial densities, slides were fixed in 10 mL of 2.5% glutaraldehyde for 20 min at room temperature, washed in Milli-Q water and air-dried. Then the slides were stained with 5 μM of SYTO13 (Invitrogen, Molecular Probes), and covered with a glass coverslip (22 × 64 mm, VWR International) for quantification of attached bacteria. After 10 min of incubation in the dark, the number of attached bacteria was determined using an AxioVision 4 image analysis system attached to a Zeiss epifluorescence microscope (40× objective; λ excitation and emission: 450/490 and 515/565 nm, respectively) and a video camera. A total of 30 measurement spots were taken at every 5 mm along three parallel rows on each slide.

Settlement and Adhesion Strength of Spores of Ulva linza. Six replicates of poly(HEMA-*co*-PEG_{10}MA) with four different thicknesses (100, 200, 400 and 600 Å) were used. In addition, six replicates each of hydrophobic CH_3 SAMs and Nexterion glass slides were also used as reference coatings. Prior to the assay, samples were equilibrated in artificial seawater (ASW) for 1 h. Standard protocols were used to measure the settlement and adhesion strength of spores of the green macroalga (seaweed) *U. linza*. In brief, motile spores (zoospores) were released from fertile plants of *U. linza* collected from Llantwit Major beach, Wales, U.K. (51° 40′ N; 3° 48′ W) as described by Callow et al.[43] and Thome et al.[44] Three replicates of each test surface were placed separately in polystyrene Quadriperm dishes (Greiner Bio-One Ltd.) and 10 mL of spores suspension with $OD_{600\ nm}$ = 0.15 (1.0 × 10^6 spores ml^{-1}) were added. Zoospores were allowed to settle for 45 min in the dark. The slides were then washed with ASW to remove unsettled (swimming) spores. To evaluate the spore densities, three slides of each test surfaces were fixed in 10 mL of 2.5% glutaraldehyde for 20 min at room temperature, washed in Milli-Q water and air-

dried. The number of settled (adhered) spores was determined by chlorophyll autofluorescence using epifluorescence microscopy (20× objective; λ excitation and emission: 546 and 590 nm, respectively) as described above.

The adhesion strength of spores was evaluated by exposing three remaining slides to a wall shear stress of 52 Pa for 5 min in a calibrated water channel.[45] After exposure to flow, slides were fixed and the spore density on all slides was determined as previously described. The number of spores remaining after exposure to flow was compared with unexposed samples as a measure of the adhesion strength of spores for each test surface.

Static Immersion Field Test. Six replicates of four different thicknesses (100, 200, 400 and 600 Å) of poly(HEMA-*co*-$PEG_{10}MA$) were randomly arranged on three different PVC panels. CH_3 SAM and Nexterion glass slides were used as references. The panels were then immersed at a static immersion test site in Hartlepool Marina, U.K. They were immersed vertically facing east and held at about 50 cm below the water level. Panels were observed, and fouling coverage was estimated at 1, 2 and 8 weeks after immersion. The fouling community was assessed in four fouling categories: microfouling, weeds, soft-bodied animals and hard-bodied animals. The percentage of each category was calculated relative to the total area of the surface. Total percentage of fouling was determined as the total percentage (sum) of these four biofouling categories.

Statistical Analysis. The adsorption of fibrinogen is presented as the thickness of fibrinogen layer adsorbed on the sample surfaces. Error bars represent the standard deviation from six measurements on each sample. The settlement densities of bacteria and spores are presented as the number of settled bacteria/spores per mm^2 with 95% confidence limits. The adhesion strength of spores is presented as percentage of removal with 95% confidence limits calculated from arcsine-transformed data.

The total fouling of the static immersion field test assays is presented as percentage fouling coverage of settlement of microfouling, weeds and soft and hard-bodied animals on the sample surfaces. Error bars represent the standard deviation from six replicates on each thickness sample.

Statistical analysis of the protein adsorption, *C. marina* and *U. linza* assays, as well as the field test data was carried out using Minitab 16 statistical software, one way analysis of variance (ANOVA) with α = 5% and Tukey's HSD Post-hoc test were performed to determine the difference between samples. Values were considered significantly different from each other when p-value (p) < 0.05.

RESULTS AND DISCUSSION

Polymer Characterization and Stability Test. A series of different thicknesses of random poly(HEMA-*co*-$PEG_{10}MA$) copolymers were prepared via SI-ATRP by varying the polymerization reaction times. The thicknesses of dry polymer films on gold substrates were measured by ellipsometry, and polymer thickness increased rapidly at first, but then the growth rate was found to decrease continuously as the polymerization proceeded (Figure 2). After 4 h, the thickness was 600 Å, but reached 1000 Å after 12−14 h. This decrease of growth rate may be due to the diminishing availability of monomer and initiator, loss of catalysts, termination of reaction or hindrance of mass transport between monomer and radical.[30] The chemical structure of different thicknesses of poly(HEMA-*co*-$PEG_{10}MA$) was characterized by IRAS (Figure 3). The presence of the HEMA and $PEG_{10}MA$ segments could be ascertained from their O—H- bond stretching, which absorbs in a broad band at 3200−3600 cm^{-1}, and which is absent from the spectrum of the initiator SAM. The C—H-stretch region (3000−2800 cm^{-1}) is dominated by the asymmetric and symmetric CH_2 stretches in PEG at 2946 and 2881 cm^{-1}, respectively. The ester carbonyl (C═O) stretching at 1732 cm^{-1}, and the skeletal PEG C—O—C stretches at 1160 and

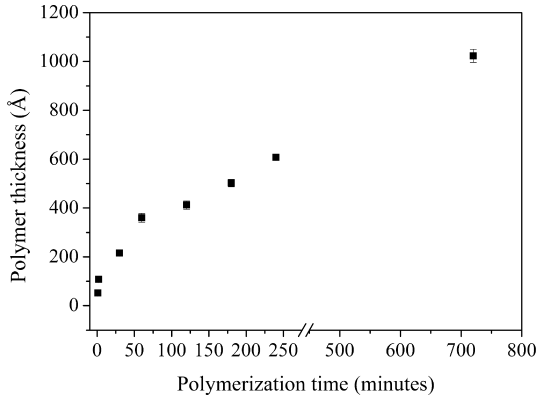

Figure 2. Ellipsometric dry thicknesses of poly(HEMA-*co*-$PEG_{10}MA$) films prepared via the SI-ATRP process, versus the reaction times.

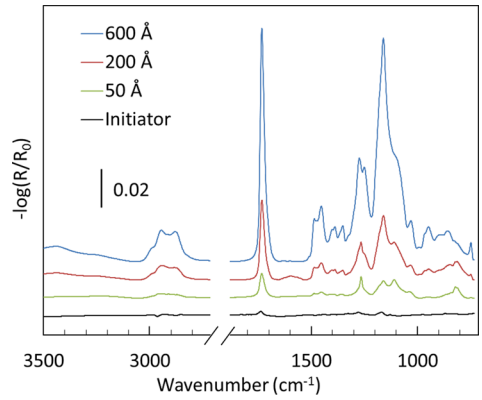

Figure 3. Infrared reflection−absorption spectra of poly(HEMA-*co*-$PEG_{10}MA$) films of different thicknesses, as well as the spectrum for the initiator SAM layer, for comparison.

1100 cm^{-1}, dominate the low-frequency end of the spectrum, and are present both in the spectra of the initiator SAM and poly(HEMA-*co*-$PEG_{10}MA$). The fingerprint region, below 1500 cm^{-1}, also contains a series of peaks from methylene deformation modes, for which detailed peak assignment is difficult and somewhat beyond the scope of this paper. The intensities of both the O—H and C—H stretch and the carbonyl bands increased with poly(HEMA-*co*-$PEG_{10}MA$) thickness, but while the O—H stretch could be affected by adsorbed water in the film (which is difficult to control even though measurements are performed under N_2 purging), the other two can be used for quantitative assessment of the amount of polymer. Integration of the carbonyl stretch band over the range 1850−1650 cm^{-1}, yields a linear relationship between ellipsometric (dry) thickness and carbonyl intensity (see Figure S1, Supporting Information), showing that the thickness increase was indeed a direct result of added polymer to the surface. These results show that poly(HEMA-*co*-$PEG_{10}MA$) was successfully polymerized from the initiator-SAM on the gold surface, and that the ellipsometric dry thickness is a very good indicator of the amount of polymerized material on the surface. In addition, the linear relation between the carbonyl peak intensity and the thickness (Figure S1, Supporting Information) also shows that there is no large difference in composition with thickness. Each monomer contributes one carbonyl moiety, whether it is HEMA or $PEG_{10}MA$, but the volume of $PEG_{10}MA$ is considerably larger than that of HEMA, and if there was a difference in

Table 1. Results of the Polymer Stability Test for Different Thicknesses of Poly(HEMA-*co*-$PEG_{10}MA$), Assessed by Static Contact Angle and Ellipsometric Measurements of Dry Film Thickness[a]

	initial condition		after 1 week		after 3 months	
nominal thickness (Å)	thickness (Å)	contact angle (θ)	thickness (Å)	contact angle (θ)	thickness (Å)	contact angle (θ)
50	51 ± 1	52 ± 1	51 ± 2	50 ± 0.4	45 ± 4	53 ± 0
100	108 ± 9	52 ± 1	108 ± 10	52 ± 2	98 ± 12	54 ± 2
200	201 ± 6	49 ± 1	202 ± 6	50 ± 1	189 ± 7	53 ± 1
400	412 ± 7	48 ± 1	411 ± 4	48 ± 2	402 ± 4	52 ± 1
600	608 ± 12	51 ± 2	608 ± 10	52 ± 0	602 ± 10	53 ± 0
1000	995 ± 8	52 ± 0	993 ± 9	51 ± 2	983 ± 9	55 ± 1

[a]Errors represent standard deviations.

composition with thickness, for example, caused by more rapid diffusion of HEMA, the relation in the figure would not be linear. Thus, we infer from this that the composition of the copolymer is homogeneous throughout the thickness of the films.

The polymer stability test, measuring thickness and wettability changes after 1, 2 and 12 weeks of immersion in ASW, shows that only minor changes in thickness and water contact angles were observed on the samples, (Table 1). There was no sign of degradation or delamination of poly(HEMA-*co*-$PEG_{10}MA$) after 1 week of incubation, demonstrating that the polymer has good short-term stability in seawater. However, after 3 months of immersion, a slight decrease of film thicknesses and small increases of water contact angles were found. Although the changes are in many cases within the measurement errors, a difference over time is expected as a consequence of oxidative degradation of PEG chains after long exposure to seawater. These results, showing good short- and long-term stability of poly(HEMA-*co*-$PEG_{10}MA$) films are in agreement with a previous study[14] on the stability of PEG-based polymer films prepared via self-initiated photografting and photopolymerization (SI-PGP).

The surface roughness and topography of dry poly(HEMA-*co*-$PEG_{10}MA$) films were observed by tapping-mode AFM in air (Figure 4). The root-mean-square (RMS) roughness of the dry films with four different thicknesses (50, 200, 600 and 1000 Å) measured over a 5 × 5 μm area with a scan rate of 1 Hz were

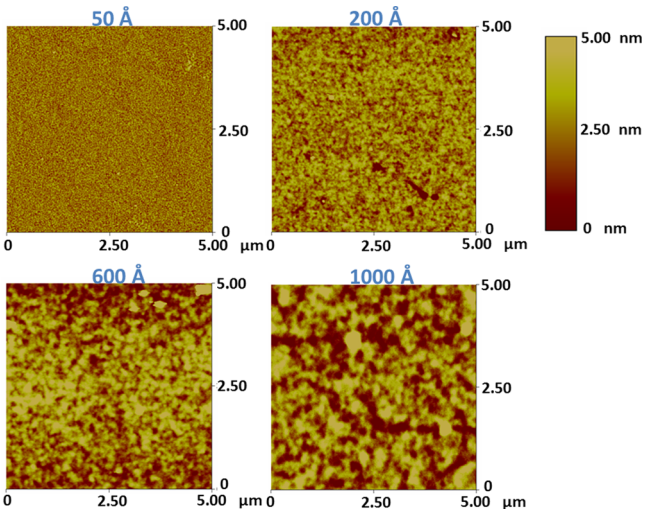

Figure 4. Topographical images of poly(HEMA-*co*-$PEG_{10}MA$) brushes of different thicknesses measured over a 5 × 5 μm area by tapping mode AFM in air. The height scale is the same in all images.

0.511, 0.784, 1.435 and 6.096 nm, respectively. The roughness of the polymers at thicknesses up to 600 Å was relatively small, suggesting that growth of the polymer up to 600 Å is well-ordered and homogeneous over the surface. The significantly higher roughness at 1000 Å might be the result of increasing chain entanglement and heterogeneity in the polymer as the chain length increases. To what extent these numbers, obtained on dry films in air, are relevant for the swollen polymer in water is unclear, but there is reason to believe that the morphological changes with thickness observed in Figure 4 also reflect a coarsening of the polymer surface with thickness also in its hydrated state under water. The poly(HEMA-*co*-$PEG_{10}MA$) film is strongly hydrated, and with a high water content in a flexible hydrophilic polymer, the surface tension would contribute to drying the polymer to a smooth surface. That this is not observed suggests that entanglement of the chains is severe, and that it provides stiffness to the topographical features seen in Figure 4 also as the film is immersed in water. This is of interest, because roughness, in general, increases the adhesion of biomacromolecules such as proteins and polysaccharides, as well as metabolites or adhesives secreted by fouling organisms,[46] and the explicit effect of roughness on the fouling would be an interesting hypothesis for future exploration of these materials.

Biofouling Assays. When a surface is exposed to natural waters, organic compounds quickly adsorb and condition the surface, and might thus provide favorable conditions or nutrients for the attachment and settlement of microbes or other propagules for further colonization. Although the role of conditioning on the settlement of fouling organisms has been widely debated, a significant impact of surface conditioning on settlement and adhesion of bacteria and some fouling organisms has been shown for some surfaces.[44,47,48] Understanding how organic material such as proteins interact and adsorb onto surfaces is important in itself, in order to study correlations with the settlement and adhesion of marine fouling organisms, which frequently use proteinaceous adhesives, or for understanding how macromolecules act to induce gregarious settlement or metamorphosis.[49] Surface resistance to non-specific protein adsorption is also essential for development of biomaterials and biomedical devices.

To study the interaction between poly(HEMA-*co*-$PEG_{10}MA$) films with proteins, an adsorption study of fibrinogen onto different thicknesses (50, 100, 200, 400 and 600 Å) of poly(HEMA-*co*-$PEG_{10}MA$) was performed, with CH_3 SAMs used as positive controls. Ellipsometric fibrinogen thicknesses on poly(HEMA-*co*-$PEG_{10}MA$) were 10−20 Å (Figure 5), much lower than adsorption to the CH_3 SAM (58 ± 8.9 Å). This is in agreement with what has been reported previously,[32,50] i.e., that lower protein adsorption was found on hydrophilic poly-

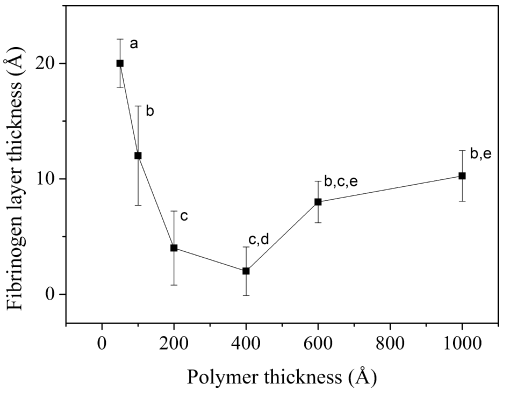

Figure 5. Adsorption of fibrinogen on different thicknesses of poly(HEMA-*co*-$PEG_{10}MA$), measured after 1 h of incubation in protein solution. The error bars represent the standard deviation from six measurements on each sample. Letters a–e indicate data points that do not differ significantly from each other at $p < 0.05$.

(HEMA-*co*-$PEG_{10}MA$) than on the hydrophobic CH_3 SAM. However, a closer look at the adsorption of fibrinogen on different thicknesses of poly(HEMA-*co*-$PEG_{10}MA$) shows that the adsorption has a minimum in the polymer thickness within the range 200–400 Å, where the adsorbed amount is lower (2–4 Å) than that on either thinner or thicker films.

In the attachment study of the marine bacterium *C. marina*, four different thicknesses (100, 200, 400 and 600 Å) of poly(HEMA-*co*-$PEG_{10}MA$) were used. The result again shows lower attachment of bacterial cells for the samples with a thickness of 200 and 400 Å (Figure 6), although the result is not as clear as for the fibrinogen assay.

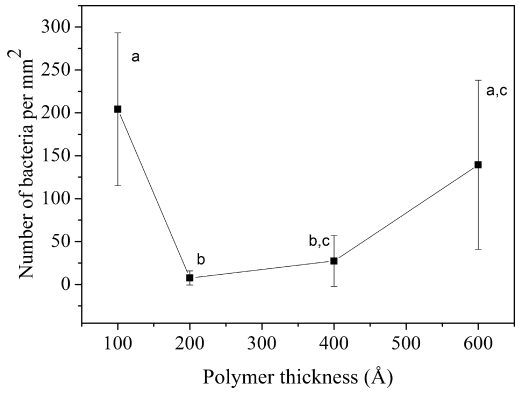

Figure 6. Attachment of marine bacterium *Cobetia marina* on four different thicknesses of poly(HEMA-*co*-$PEG_{10}MA$). Error bars represent ±2 × SE calculated from arcine-transformed data. Letters a–c indicate data points that do not differ significantly from each other at $p < 0.05$.

In the study of settlement and adhesion strength of the marine alga *U. linza* with the same four thicknesses (100, 200, 400 and 600 Å) of poly(HEMA-*co*-$PEG_{10}MA$), relatively high settlement of spores was observed on the lowest (100 Å) and highest (600 Å) thicknesses, whereas the lowest settlement of spores was found on the 200 and 400 Å thick samples (Figure 7). Statistical analysis confirmed that the number of settled spores on all samples differed significantly, except at the thicknesses 200 and 400 Å ($p < 0.05$). Furthermore, the spore adhesion strength study also revealed that the adhesion strength of settled spores is weakest for the samples with

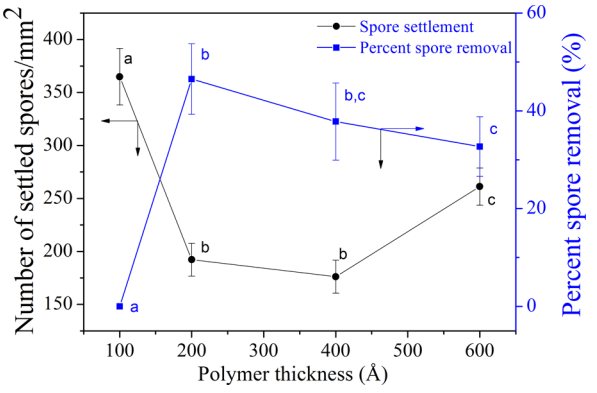

Figure 7. Settlement of spores of *U. linza* on four different thicknesses of poly(HEMA-*co*-$PEG_{10}MA$) and percent removal after exposure to 52 Pa shear stress. Error bars represent ±2 × SE calculated from arcsine-transformed data with 95% confidence limit. Letters a–c for each curve indicate data points that do not differ significantly from each other at $p < 0.05$.

least settlement, which is seen as a higher percentage of removed spores after exposure to a shear stress of 52 Pa in a flow channel (see Figure 7). In combination, this lower settlement and higher removal on thicknesses 200 and 400 Å indicates that the adhesion of spores in this range is unfavorable.

Static immersion field tests confirmed that total fouling was lower on the 200 and 400 Å thick polymer films after 2 weeks of immersion in seawater at a marina (Figure 8, see Figure S3 in

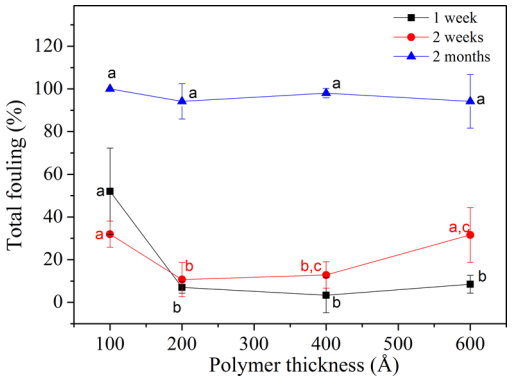

Figure 8. Percent settlement of total fouling on four different thicknesses (100, 200, 400 and 600 Å) of poly(HEMA-*co*-$PEG_{10}MA$) observed after 1 (squares), 2 (circles) and 8 (triangles) weeks of immersion in seawater at the depth 0.5 m below sea level. Error bars represent standard deviation from six replicates of each sample. Letters indicate data points that do not differ significantly from each other at $p < 0.05$.

the Supporting Information for photographs of the samples). However, after longer immersion (2 months) in seawater, all of the samples were fully covered by fouling organisms, probably a consequence of oxidative degradation of PEG chains or mechanical instability of the polymer or the gold layers under the influence of water currents and variations in temperature and salinity.

We hypothesize that the lower fouling and adhesion within the thickness range 200–400 Å can be associated with physicochemical properties of hydrated polymer chains. Unlike hydrophilic nonfouling SAMs, where chain viscoelasticity plays a little role in determining their antifouling properties due to

higher packing density and shorter chains, antifouling properties of longer chain polymers are also influenced by bulk hydration and viscoelastic properties.[51] When hydrophilic polymers contact bulk water, water molecules infiltrate into the film hydrogen-bond strongly to polar moieties along the chains, forming a hydrogen-bond network and a hydrated polymer brush. The enthalpic cost of displacing this hydration water aids in preventing the attachment of proteins or fouling organisms.[52−54] However, polymer chains expanded by hydration will change their mechanical properties and exhibit both viscous and elastic properties in water. Therefore, to investigate the role of brush viscoelasticity, QCM studies of brush hydration were conducted.

Wet Properties of Poly(HEMA-co-PEG$_{10}$MA): Hydration and Polymer Viscoelasticity. Understanding chain conformation of hydrated polymers at interfaces, and how it influences polymer physicochemical properties, is essential to understand and improve polymer antifouling properties. Quartz crystal microbalance with dissipation (QCM-D) is a technique that can be used for studying the hydration and viscoelasticity of hydrated polymer brushes at solid−water interfaces. According to the Sauerbrey equation,[55] the added mass to an oscillating sensor crystal (Δm) is proportional to the change of resonance frequency (Δf):

$$\Delta m = -C\frac{1}{n}\Delta f$$

where Δf is the change in frequency at the n^{th} overtone, and C is a proportionality constant of the QCM-D crystal. In this work, crystals with nominal frequency of 4.950 MHz and C = 0.177 mg/m^2 were used. The change of dissipation factor (ΔD) is defined by

$$\Delta D = \frac{E_d}{2\pi E_s}$$

where E_d is energy dissipated during one oscillation and E_s is the energy stored in the oscillating system. The change in dissipation factor (ΔD) can be associated with the viscoelasticity of an adsorbed layer on the sensor crystal.

In this work, the change of frequency (Δf) and dissipation (ΔD) were observed at three overtones (3rd, 5th and 7th). Only results for Δf and ΔD at the 3rd overtone are shown here because all three overtones show an identical trend of Δf and ΔD. The Δf and ΔD data were measured both on uncoated (reference) and polymer-coated sensor crystals, and the frequency and dissipation difference measured between uncoated and polymer-coated crystals was defined as Δf_{film} and ΔD_{film}. Here we also demonstrated that the calculation of Δf_{film} and ΔD_{film} by the Voigt model predicts the same trends as the measured data. The presented data was obtained on polymer films immersed in Milli-Q water, but the swelling of the polymer does not change in PBS or ASW (see Figure S4, Supporting Information), as would be expected for an uncharged and strongly hydrated polymer. The magnitude of the frequency change (Δf_{film}), normalized by the ellipsometric dry polymer thickness, significantly changes at 200 Å and reaches a maximum negative value at 300 Å thickness, and then gradually decreases again as the thickness increases further (Figure 9). This result indicates that as the polymer is made thicker, the mass per polymer segment increases to a maximum at 300 Å. This difference in added mass as the polymer is made thicker can only come from hydration water trapped in the film,

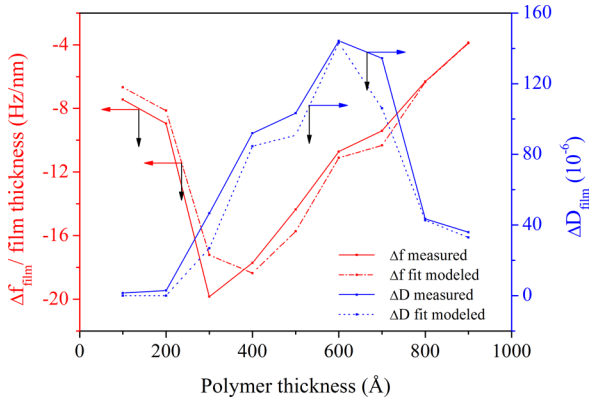

Figure 9. Measured and calculated data for the frequency change (Δf_{film}) normalized by the film thickness and dissipation change (ΔD_{film}) of hydrated poly(HEMA-*co*-PEG$_{10}$MA) measured by QCM-D. The calculated data (dotted/dashed lines) were obtained using the output parameters (Table S1, Supporting Information) from fitting a one-layer viscoelastic Voigt model to the experimental data of both Δf and ΔD.

which is thus most strongly hydrated at this thickness. This is confirmed by the hydrated thicknesses, as obtained from the Voigt model fitting (Figure 10), showing that the swelling of

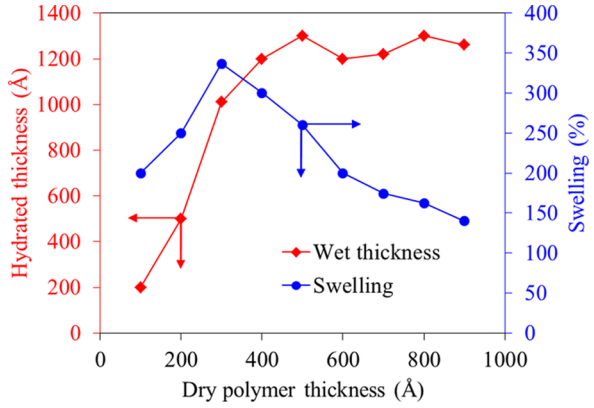

Figure 10. Hydrated thickness (diamonds, left ordinate) of the polymer films, as obtained from the modeling of the QCM-D data in the Voigt model, yielding the acoustic thickness in a slab model. For fit parameters, see Table S1 (Supporting Information). Also shown is the relative swelling (circles, right ordinate) due to water uptake.

the film is greatest at 300 Å (dry) thickness. Higher hydration suggests higher availability of hydrogen-forming moieties, but because the local structure of the polymer chain is expected to be the same throughout the thickness of the brush, any difference in hydration is expected to stem from chain conformation differences and chain−chain interactions. For the smallest thicknesses, we infer that the total hydration of the surface is too low for it to display good antifouling properties, though it should be noted that in absolute terms, the antifouling properties are fairly good. Compare, for example, the adsorbed fibrinogen amount with the CH_3 SAM positive control. For intermediate thicknesses, hydration (per unit added polymer) is largest, resulting in a strongly hydrated and fouling-resistant brush. As the thickness increases to above 600 Å, hydration is significantly reduced, presumably due to increasing entanglement as a result of crowding, and stronger inter- and intrachain interaction, leading to reduced availability

of hydrogen-bonding functional groups, higher density of polymer chains and reduced hydration. The hydrated thickness increases for dry thicknesses up to 400−500 Å, but levels out to a constant thickness beyond that, so that while more polymer is added to the film, this does not lead to a further increase in hydrated thickness (Figure 10), which must then result in higher polymer density and less available space for hydration. This observation is in accordance with established knowledge and the general observation that hydration is important in determining antifouling properties of hydrophilic polymers; Chen et al.[51] have reported that higher surface hydration on hydrophilic polymer films results in nonfouling properties and that any reduction in surface hydration might lead to a decrease in its nonfouling properties due to increase of packing density, increase of hydrophobicity when copolymerized with hydrophobic monomers and rise of temperature.

The measured dissipation was found to change gradually, and increased at thicknesses from 200 Å, to reach a maximum at 600 Å, and then significantly decreased again (Figure 9), suggesting that the hydrated polymer films tend to be relatively stiff at thicknesses less than 200 Å and higher than 800 Å. Modeling of the viscoelastic properties of the film revealed clear variations in these over the thickness range 200−900 Å. The viscoelasticity has two contributions; viscosity represents the resistance to gradual deformation by shear or tensile stress, whereas elasticity represents the relaxation flexibility in response to stress. As shown in Figure 11, the viscosity of

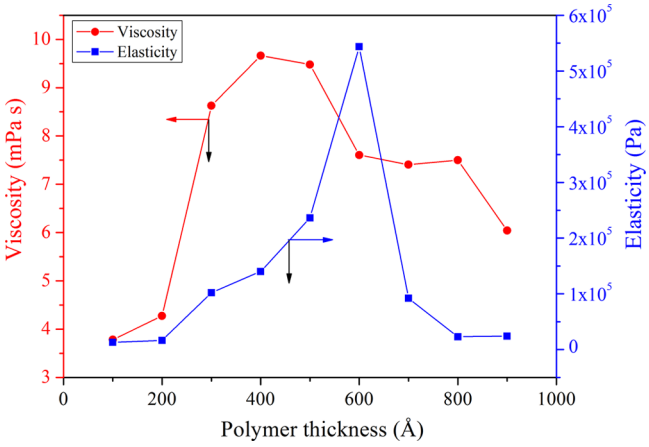

Figure 11. Viscosity and elasticity of hydrated poly(HEMA-*co*-$PEG_{10}MA$) films, as obtained by fitting the data from Figure 9 to a one-layer viscoelastic Voigt model, using the parameters in Table S1 (Supporting Information).

the polymer layers increased significantly at 200 Å and decreased gradually beyond 500 Å. The highest viscosity was achieved in the thickness range 300−500 Å. This result indicates larger number of water molecules bound to the polymer chains, i.e. larger swelling, due to a higher degree of hydrogen-bond formation on or around the polymer chains. Polymers in this thickness range are thus expected to exhibit the most prominent antifouling characteristics, in agreement with the experimental results. Figure 11 also shows that the polymer elasticity peaked at 600 Å. Higher elasticity indicates a higher ability of the polymer film to return to its original shape after an applied force is removed. At thicknesses less than 200 Å the short chain length makes the polymer stiff. The higher elasticity within 500−700 Å might be due to longer chains; however, when the chain length increases further, the elasticity decreases due to higher chain entanglement. As the polymerization proceeds, reduced availability of monomer and initiator, loss of catalysts, termination reactions or mass transport hindrance will increase the number of defects and reduce the number of "living" chains near the surface of the film and contribute to surface heterogeneity. This may also affect the adsorption to the surface, but the clear reduction both in dissipation and elasticity for thicknesses beyond 600 Å shows that there is a considerable change in bulk properties of the film at increasing thickness, indicating that increasing entanglement of the chains is the dominating effect of the increased polymerization time. In a recent AFM study of the relation between surface elasticity and protein repellency, Inoue et al. found a strong suppression of protein−surface interactions at surfaces with high elastic repulsion, resulting from dense polymer brush structures.[56] Although viscous and elastic responses from the polymer film were not distinguished in that study (but the elastic response derived directly from the dynamic repulsion energy), we see a qualitative similarity in that our samples with greatest viscoelastic response also were those that most effectively reduced fouling. This is also a central point where the mechanism of protein resistance relies on expulsion of the protein from the film due to osmotic stress in a dehydrated brush,[57] and would thus support the view that it is bulk hydration and water uptake in the polymer that is responsible for the effective antifouling properties in our case, and not strong surface hydration, which appears to be responsible for protein resistance in SAMs with small hydrophilic functional groups.

Surface Energy. To investigate whether the differences in hydration and viscoelastic properties were also associated with changes in surface energy, the surface energy of hydrated poly(HEMA-*co*-$PEG_{10}MA$) was determined by measuring captive-bubble contact angles of air and *n*-octane, and using the Owens and Wendt approach to calculate the energies. As shown in Figure 12, surface energies of hydrated poly(HEMA-

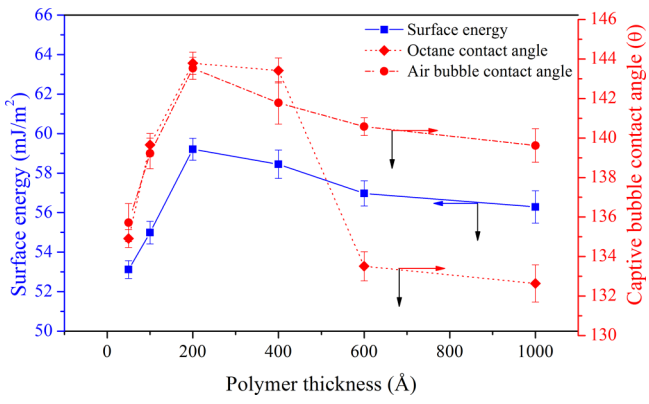

Figure 12. Surface energy of hydrated poly(HEMA-*co*-$PEG_{10}MA$) calculated from the captive-bubble contact angles of water and *n*-octane, measured in Milli-Q water.

co-$PEG_{10}MA$) fall in the range 53−59 mJ/m^2. We note again that there is a variation of surface properties over the tested range of thicknesses, and although the variation in surface energy is relatively small, it is interesting that there is a maximum around the thicknesses of 200 and 400 Å. This is consistent with the observed differences in hydration; a relative increase in water content at these thicknesses would increase

the surface free energy relative to that of the polymer (the dry polymer is not readily wetted and thus much less polar than water. Advancing contact angles in air of the polymers are approximately 60°, see Figure S2 in the Supporting Information). Surface energy is an important parameter to consider in bioadhesion and biofouling. Some reports on the influence of surface energy on bioadhesion have shown minima in bacterial adhesion around 20−30 mJ/m^2.[58−61] However, others have demonstrated that the adhesion of bacteria and barnacle cyprids do not strongly correlate with surface energy,[18,24,62] and we show in this case, that trends in settlement and adhesion of fouling organisms cannot be determined by surface energy, and that other properties such as hydration and viscoelasticity significantly influence the resulting fouling. The adhesion of organisms to surfaces in nature is even more complex as the surfaces are immediately conditioned by biomacromolecules, altering the surface properties for further attachment.[44,63]

To summarize, we found that surface hydration and surface energy was higher for the polymer films in the thickness range 200−400 Å, where the polymer chains are highly hydrated and form dense water molecule networks. Higher viscosity and moderate elasticity within this range also contribute to the lower adhesion of proteins and fouling organisms, as a result of better steric stabilization of the chains. Furthermore, we anticipate that the smoothness of the thinner surfaces also contribute to the good antifouling properties of poly(HEMA-*co*-PEG$_{10}$MA).

The antifouling properties of poly(HEMA-*co*-PEG$_{10}$MA), in general, are strongly associated with the presence of PEG chains, which has well-known antifouling properties. Moreover, the absence of charge in the structure of poly(HEMA-*co*-PEG$_{10}$MA) prevents the surface from electrostatic interaction with proteins and other biomacromolecules secreted by fouling organisms. In this work, poly(HEMA-*co*-PEG$_{10}$MA) showed good antifouling properties and stability during short-term incubation in water. However, antifouling properties were not maintained during longer (2 months) field tests, after which almost all of the surfaces were fully covered by marine biofouling, and there was no difference between samples of different polymer thickness.

Our observations are in good agreement with previous reports on the thickness dependence of protein adsorption: Sun et al. studied fibrinogen adsorption onto graft copolymerized layers of HEMA and methoxylated PEGMA (MPEG$_4$MA), and observed a minimum in fibrinogen adsorption at a grafted amount of about 4−5 mg/cm^2.[64] Yang et al.[30] studied protein adsorption from blood serum and plasma onto poly(sulfobetaine methacrylate) (pSBMA) brushes with thicknesses from 150 to 900 Å, and found that the adsorption had a minimum for a 620 Å thick film. Zhao et al.[65] studied the correlation between protein adhesion and film thickness for poly(2-hydroxyethyl methacrylate) (pHEMA) and poly(hydroxypropyl methacrylate) (pHPMA) films, and similarly found minima in the adsorption around 200−400 Å, where the exact range differed slightly depending on the material and the protein. Although Yang et al. did not provide any explanation for the occurrence of a fouling minimum, Sun et al. concluded from electron micrographs that area enlargement due to increasing roughness was the cause of the increase in adsorption with grafted amount. Zhao et al. inferred from topography measurements by AFM that entanglement and condensation of chains in thicker films reduced hydration capacity, leading to increased protein adsorption, an argument fully supported by the data presented here. That protein adsorption minima are observed on brushes of a range of materials, i.e., poly(HEMA-*co*-MPEG$_4$MA),[64] pSBMA,[30] pHEMA and pHPMA,[65] as well as poly(HEMA-*co*-PEG$_{10}$MA) (this study), suggest that this is a phenomenon with some generality, and our results demonstrate that this is not limited to protein fouling but applies also to fouling of marine organisms. We note that the polymers listed above all have chains with functional side groups. The situation is different with PEG, which is a straight-chain polymer, for which protein resistance improves with chain length (at a given chain density), but only to some limits. After a certain length has been reached, little or no molecular-weight dependence of the resistance is observed. As an example, fibrinogen adsorption has been shown to decrease up to a PEG weight of approximately 1500 Da, but did not vary beyond this.[66] This difference points to side groups restricting the conformational freedom for polymers as the length of the backbone increases, leading to entanglement, stronger inter- and intrachain interactions, reduced hydration and thus eventually reduced antifouling efficiency. However, for poly(HEMA-*co*-PEG$_{10}$MA), it is anticipated that the bulkier PEG$_{10}$MA monomers contribute considerably to the antifouling properties,[14] and thus it will remain necessary to tune the coating thickness to optimize performance.

CONCLUSIONS

We have demonstrated the influence of polymer thickness on the antifouling properties of poly(HEMA-*co*-PEG$_{10}$MA) brushes. The important finding in this work is that there is an optimum thickness range for poly(HEMA-*co*-PEG$_{10}$MA) brushes around 200−400 Å (dry thickness), with higher resistance to fibrinogen adsorption, and to the settlement and adhesion of the marine bacterium *Cobetia marina*, and zoospores of the green alga *Ulva linza*. The better antifouling performance in this thickness range is related to higher polymer hydration and viscosity, and is also accompanied by an increase in surface energy. In this range of thicknesses, we also observed a reduction of marine fouling in a field test after 2 weeks, though after 2 months of immersion, this difference was eliminated, probably as a result of surface degradation. Reduced antifouling performance at thicknesses below the optimum range is presumably caused by a lower hydration capacity of the polymer, and at chain lengths increasing beyond the optimum range, entanglement and crowding in the film reduces the conformational freedom and the hydration capacity, leading to reduced antifouling properties.

ASSOCIATED CONTENT

Supporting Information

Correlation between carbonyl IR peak area and ellipsometric thickness, contact angle data for poly(HEMA-*co*-PEG$_{10}$MA) films of different thicknesses, photographs of samples after the static immersion field tests, QCM-D data for the polymer film in the different aqueous media used and parameters for the QCM-D data modeling. This material is available free of charge via the Internet at http://pubs.acs.org.

AUTHOR INFORMATION

Corresponding Author

*T. Ederth. E-mail: ted@ifm.liu.se.

Notes

The authors declare no competing financial interest.

■ ACKNOWLEDGMENTS

This study has received funding from the European Community's Seventh Framework Program FP7/2007−2013 under Grant Agreement number [237997] (SEACOAT). T.E. acknowledges financial support from the Swedish Government Strategic Research Area in Materials Science on Functional Materials at Linköping University (Faculty Grant SFO-Mat-LiU # 2009-00971).

■ REFERENCES

(1) Hellio, C.; Yebra, D. *Advances in Marine Antifouling Coatings and Technologies*, 1 ed.; Woodhead Publishing Limited and CRC Press LLC: Cambridge, U.K., 2009.

(2) Schultz, M. P. Effects of Coating Roughness and Biofouling on Ship Resistance and Powering. *Biofouling* **2007**, *23*, 331−341.

(3) Lin, C. Y.; Chen, W. C. Effects of Potassium Sulfide Content in Marine Diesel Fuel Oil on Emission Characteristics of Marine Furnaces under Varying Humidity of Inlet Air. *Ocean Eng.* **2006**, *33*, 1260−1270.

(4) Fitridge, I.; Dempster, T.; Guenther, J.; de Nys, R. The Impact and Control of Biofouling in Marine Aquaculture: A Review. *Biofouling* **2012**, *28*, 649−669.

(5) Thomas, K. V.; Brooks, S. The Environmental Fate and Effects of Antifouling Paint Biocides. *Biofouling* **2010**, *26*, 73−88.

(6) Cheyne, I. Regulation of Marine Antifouling in International and Ec Law. In *Biofouling*; Simone Dürr, J. C. T., Ed.; Wiley-Blackwell: Chichester, U.K., 2010; pp 306−314.

(7) Callow, J. A.; Callow, M. E. Trends in the Development of Environmentally Friendly Fouling-Resistant Marine Coatings. *Nat. Commun.* **2011**, *2*.

(8) Schilp, S.; Kueller, A.; Rosenhahn, A.; Grunze, M.; Pettitt, M. E.; Callow, M. E.; Callow, J. A. Settlement and Adhesion of Algal Cells to Hexa (Ethylene Glycol)-Containing Self-Assembled Monolayers with Systematically Changed Wetting Properties. *Biointerphases* **2007**, *2*, 143−150.

(9) Ista, L. K.; Fan, H. Y.; Baca, O.; Lopez, G. P. Attachment of Bacteria to Model Solid Surfaces: Oligo(Ethylene Glycol) Surfaces Inhibit Bacterial Attachment. *Fems Microbiol. Lett.* **1996**, *142*, 59−63.

(10) Ederth, T.; Pettitt, M. E.; Nygren, P.; Du, C. X.; Ekblad, T.; Zhou, Y.; Falk, M.; Callow, M. E.; Callow, J. A.; Liedberg, B. Interactions of Zoospores of Ulva Linza with Arginine-Rich Oligopeptide Monolayers. *Langmuir* **2009**, *25*, 9375−9383.

(11) Ederth, T.; Nygren, P.; Pettitt, M. E.; Östblom, M.; Du, C. X.; Broo, K.; Callow, M. E.; Callow, J.; Liedberg, B. Anomalous Settlement Behavior of Ulva Linza Zoospores on Cationic Oligopeptide Surfaces. *Biofouling* **2008**, *24*, 303−312.

(12) Fyrner, T.; Lee, H. H.; Mangone, A.; Ekblad, T.; Pettitt, M. E.; Callow, M. E.; Callow, J. A.; Conlan, S. L.; Mutton, R.; Clare, A. S.; Konradsson, P.; Liedberg, B.; Ederth, T. Saccharide-Functionalized Alkanethiols for Fouling-Resistant Self-Assembled Monolayers: Synthesis, Monolayer Properties, and Antifouling Behavior. *Langmuir* **2011**, *27*, 15034−15047.

(13) Ederth, T.; Ekblad, T.; Pettitt, M. E.; Conlan, S. L.; Du, C. X.; Callow, M. E.; Callow, J. A.; Mutton, R.; Clare, A. S.; D'Souza, F.; Donnelly, G.; Bruin, A.; Willemsen, P. R.; Su, X. J. J.; Wang, S.; Zhao, Q.; Hederos, M.; Konradsson, P.; Liedberg, B. Resistance of Galactoside-Terminated Alkanethiol Self-Assembled Monolayers to Marine Fouling Organisms. *ACS Appl. Mater. Interfaces* **2011**, *3*, 3890−3901.

(14) Ekblad, T.; Bergström, G.; Ederth, T.; Conlan, S. L.; Mutton, R.; Clare, A. S.; Wang, S.; Liu, Y. L.; Zhao, Q.; D'Souza, F.; Donnelly, G. T.; Willemsen, P. R.; Pettitt, M. E.; Callow, M. E.; Callow, J. A.; Liedberg, B. Poly(Ethylene Glycol)-Containing Hydrogel Surfaces for Antifouling Applications in Marine and Freshwater Environments. *Biomacromolecules* **2008**, *9*, 2775−2783.

(15) Statz, A.; Finlay, J.; Dalsin, J.; Callow, M.; Callow, J. A.; Messersmith, P. B. Algal Antifouling and Fouling-Release Properties of Metal Surfaces Coated with a Polymer Inspired by Marine Mussels. *Biofouling* **2006**, *22*, 391−399.

(16) Krishnan, S.; Ayothi, R.; Hexemer, A.; Finlay, J. A.; Sohn, K. E.; Perry, R.; Ober, C. K.; Kramer, E. J.; Callow, M. E.; Callow, J. A.; Fischer, D. A. Anti-Biofouling Properties of Comblike Block Copolymers with Amphiphilic Side Chains. *Langmuir* **2006**, *22*, 5075−5086.

(17) Finlay, J. A.; Callow, M. E.; Ista, L. K.; Lopez, G. P.; Callow, J. A. The Influence of Surface Wettability on the Adhesion Strength of Settled Spores of the Green Alga Enteromorpha and the Diatom Amphora. *Integr. Comp. Biol.* **2002**, *42*, 1116−1122.

(18) Petrone, L.; Di Fino, A.; Aldred, N.; Sukkaew, P.; Ederth, T.; Clare, A. S.; Liedberg, B. Effects of Surface Charge and Gibbs Surface Energy on the Settlement Behaviour of Barnacle Cyprids (Balanus Amphitrite). *Biofouling* **2011**, *27*, 1043−1055.

(19) Callow, J. A.; Callow, M. E.; Ista, L. K.; Lopez, G.; Chaudhury, M. K. The Influence of Surface Energy on the Wetting Behaviour of the Spore Adhesive of the Marine Alga Ulva Linza (Synonym Enteromorpha Linza). *J. R. Soc., Interface* **2005**, *2*, 319−325.

(20) Kerr, A.; Beveridge, C. M.; Cowling, M. J.; Hodgkiess, T.; Parr, A. C. S.; Smith, M. J. Some Physical Factors Affecting the Accumulation of Biofouling. *J. Mar. Biol. Assoc. U. K.* **1999**, *79*, 357−359.

(21) Scardino, A. J.; Zhang, H.; Cookson, D. J.; Lamb, R. N.; de Nys, R. The Role of Nano-Roughness in Antifouling. *Biofouling* **2009**, *25*, 757−767.

(22) Chaudhury, M. K.; Finlay, J. A.; Chung, J. Y.; Callow, M. E.; Callow, J. A. The Influence of Elastic Modulus and Thickness on the Release of the Soft-Fouling Green Alga Ulva Linza (Syn. Enteromorpha Linza) from Poly(Dimethylsiloxane) (PDMS) Model Networks. *Biofouling* **2005**, *21*, 41−48.

(23) Yarbrough, J. C.; Rolland, J. P.; DeSimone, J. M.; Callow, M. E.; Finlay, J. A.; Callow, J. A. Contact Angle Analysis, Surface Dynamics, and Biofouling Characteristics of Cross-Linkable, Random Perfluoropolyether-Based Graft Terpolymers. *Macromolecules* **2006**, *39*, 2521−2528.

(24) Di Fino, A.; Petrone, L.; Aldred, N.; Ederth, T.; Liedberg, B.; Clare, A. S. Correlation between Surface Chemistry and Settlement Behaviour in Barnacle Cyprids (*Balanus Improvisus*). *Biofouling* **2014**, *30*, 143−152.

(25) Prendergast, G. S. Settlement and Behaviour of Marine Fouling Organisms. In *Biofouling*; Simone Dürr, J. C. T., Ed.; Wiley-Blackwell: Chichester, U.K, 2010; pp 30−59.

(26) Jiang, S. Y.; Cao, Z. Q. Ultralow-Fouling, Functionalizable, and Hydrolyzable Zwitterionic Materials and Their Derivatives for Biological Applications. *Adv. Mater. (Weinheim, Ger.)* **2010**, *22*, 920−932.

(27) Jeon, S. I.; Lee, J. H.; Andrade, J. D.; Degennes, P. G. Protein Surface Interactions in the Presence of Polyethylene Oxide .1. Simplified Theory. *J. Colloid Interface Sci.* **1991**, *142*, 149−158.

(28) Jeon, S. I.; Andrade, J. D. Protein Surface Interactions in the Presence of Polyethylene Oxide 2. Effect of Protein Size. *J. Colloid Interface Sci.* **1991**, *142*, 159−166.

(29) Feng, W.; Zhu, S. P.; Ishihara, K.; Brash, J. L. Protein Resistant Surfaces: Comparison of Acrylate Graft Polymers Bearing Oligo-Ethylene Oxide and Phosphorylcholine Side Chains. *Biointerphases* **2006**, *1*, 50−60.

(30) Yang, W.; Chen, S. F.; Cheng, G.; Vaisocherova, H.; Xue, H.; Li, W.; Zhang, J. L.; Jiang, S. Y. Film Thickness Dependence of Protein Adsorption from Blood Serum and Plasma onto Poly(sulfobetaine)-Grafted Surfaces. *Langmuir* **2008**, *24*, 9211−9214.

(31) Wendt, D. E.; Kowalke, G. L.; Kim, J.; Singer, I. L. Factors That Influence Elastomeric Coating Performance: The Effect of Coating Thickness on Basal Plate Morphology, Growth and Critical Removal Stress of the Barnacle Balanus Amphitrite. *Biofouling* **2006**, *22*, 1−9.

(32) Larsson, A.; Ekblad, T.; Andersson, O.; Liedberg, B. Photografted Poly(ethylene Glycol) Matrix for Affinity Interaction Studies. *Biomacromolecules* **2007**, *8*, 287−295.
(33) Ma, H. W.; Hyun, J. H.; Stiller, P.; Chilkoti, A. "Non-Fouling" Oligo(ethylene Glycol)-Functionalized Polymer Brushes Synthesized by Surface-Initiated Atom Transfer Radical Polymerization. *Adv. Mater. (Weinheim, Ger.)* **2004**, *16*, 338−341.
(34) Chang, Y.; Chen, W. Y.; Yandi, W.; Shih, Y. J.; Chu, W. L.; Liu, Y. L.; Chu, C. W.; Ruaan, R. C.; Higuchi, A. Dual-Thermoresponsive Phase Behavior of Blood Compatible Zwitterionic Copolymers Containing Nonionic Poly(N-Isopropyl Acrylamide). *Biomacromolecules* **2009**, *10*, 2092−2100.
(35) Li, B.; Yu, B.; Huck, W. T. S.; Zhou, F.; Liu, W. M. Electrochemically Induced Surface-Initiated Atom-Transfer Radical Polymerization. *Angew. Chem., Int. Ed.* **2012**, *51*, 5092−5095.
(36) Hui, C. M.; Pietrasik, J.; Schmitt, M.; Mahoney, C.; Choi, J.; Bockstaller, M. R.; Matyjaszewski, K. Surface-Initiated Polymerization as an Enabling Tool for Multifunctional (Nano-)Engineered Hybrid Materials. *Chem. Mater.* **2014**, *26*, 745−762.
(37) Owens, D. K.; Wendt, R. C. Estimation of the Surface Free Energy of Polymers. *J. Appl. Polym. Sci.* **1969**, *13*, 1741−1747.
(38) Roudman, A. R.; DiGiano, F. A. Surface Energy of Experimental and Commercial Nanofiltration Membranes: Effects of Wetting and Natural Organic Matter Fouling. *J. Membr. Sci.* **2000**, *175*, 61−73.
(39) Cobet, A. B.; Wirsen, C.; Jones, G. E. The Effect of Nickel on a Marine Bacterium, *Arthrobacter Marinus* Sp. Nov. *J. Gen. Microbiol.* **1970**, *62*, I 59−1 69.
(40) Arahal, D. R.; Castillo, A. M.; Ludwig, W.; Schleifer, K. H.; Ventosa, A. Proposal of Cobetia Marina Gen. Nov., Comb. Nov., within the Family Halomonadaceae, to Include the Species Halomonas Marina. *Syst. Appl. Microbiol.* **2002**, *25*, 207−211.
(41) Mieszkin, S.; Martin-Tanchereau, P.; Callow, M. E.; Callow, J. A. Effect of Bacterial Biofilms Formed on Fouling-Release Coatings from Natural Seawater and Cobetia Marina, on the Adhesion of Two Marine Algae. *Biofouling* **2012**, *28*, 953−68.
(42) Pranzetti, A.; Salaun, S.; Mieszkin, S.; Callow, M. E.; Callow, J. A.; Preece, J. A.; Mendes, P. M. Model Organic Surfaces to Probe Marine Bacterial Adhesion Kinetics by Surface Plasmon Resonance. *Adv. Funct. Mater.* **2012**, *22*, 3672−3681.
(43) Callow, M. E.; Callow, J. A.; Pickett-Heaps, J. D.; Wetherbee, R. Primary Adhesion of Enteromorpha Propagules. *Phycologia* **1997**, *36*, 15−15.
(44) Thome, I.; Pettitt, M. E.; Callow, M. E.; Callow, J. A.; Grunze, M.; Rosenhahn, A. Conditioning of Surfaces by Macromolecules and Its Implication for the Settlement of Zoospores of the Green Alga Ulva Linza. *Biofouling* **2012**, *28*, 501−510.
(45) Schultz, M. P.; Finlay, J. A.; Callow, M. E.; Callow, J. A. A Turbulent Channel Flow Apparatus for the Determination of the Adhesion Strength of Microfouling Organisms. *Biofouling* **2000**, *15*, 243−251.
(46) Vladkova, T. Surface Modification Approach to Control Biofouling. In *Marine and Industrial Biofouling*; Flemming, H.-C. Murthy, P. S., Venkatesan, R., Cooksey, K. E., Eds.; Springer: Berlin, 2009.
(47) Muller, W. E. G.; Wang, X. H.; Proksch, P.; Perry, C. C.; Osinga, R.; Garderes, J.; Schroder, H. C. Principles of Biofouling Protection in Marine Sponges: A Model for the Design of Novel Biomimetic and Bio-Inspired Coatings in the Marine Environment? *Mar. Biotechnol.* **2013**, *15*, 375−398.
(48) Kirschner, C. M.; Brennan, A. B. Bio-Inspired Antifouling Strategies. *Annu. Rev. Mater. Res.* **2012**, *42*, 211−229.
(49) Burke, R. D. Pheromones and the Gregarious Settlement of Marine Invertebrate Larvae. *B. Mar. Sci.* **1986**, *39*, 323−331.
(50) Faxälv, L.; Ekblad, T.; Liedberg, B.; Lindahl, T. L. Blood Compatibility of Photografted Hydrogel Coatings. *Acta Biomater.* **2010**, *6*, 2599−2608.
(51) Chen, S. F.; Li, L. Y.; Zhao, C.; Zheng, J. Surface Hydration: Principles and Applications toward Low-Fouling/Nonfouling Biomaterials. *Polymer* **2010**, *51*, 5283−5293.
(52) He, Y.; Hower, J.; Chen, S. F.; Bernards, M. T.; Chang, Y.; Jiang, S. Y. Molecular Simulation Studies of Protein Interactions with Zwitterionic Phosphorylcholine Self-Assembled Monolayers in the Presence of Water. *Langmuir* **2008**, *24*, 10358−10364.
(53) Morisaku, T.; Watanabe, J.; Konno, T.; Takai, M.; Ishihara, K. Hydration of Phosphorylcholine Groups Attached to Highly Swollen Polymer Hydrogels Studied by Thermal Analysis. *Polymer* **2008**, *49*, 4652−4657.
(54) Shao, Q.; He, Y.; White, A. D.; Jiang, S. Y. Difference in Hydration between Carboxybetaine and Sulfobetaine. *J. Phys. Chem. B* **2010**, *114*, 16625−16631.
(55) Sauerbrey, G. Verwendung Von Schwingquarzen Zur Wägung Dünner Schichten Und Zur Mikrowägung. *Zeitschrift für Physik* **1959**, *155*, 206−222.
(56) Inoue, Y.; Nakanishi, T.; Ishihara, K. Elastic Repulsion from Polymer Brush Layers Exhibiting High Protein Repellency. *Langmuir* **2013**, *29*, 10752−10758.
(57) Halperin, A. Polymer Brushes That Resist Adsorption of Model Proteins: Design Parameters. *Langmuir* **1999**, *15*, 2525−2533.
(58) Dexter, S. C. Influence of Substratum Critical Surface-Tension on Bacterial Adhesion—In Situ Studies. *J. Colloid Interface Sci.* **1979**, *70*, 346−354.
(59) Baier, R. E.; Meyer, A. E. Surface Analysis of Fouling-Resistant Marine Coatings. *Biofouling* **1992**, *6*, 165−180.
(60) Zhao, Q. Effect of Surface Free Energy of Graded Ni-P-Ptfe Coatings on Bacterial Adhesion. *Surf. Coat. Technol.* **2004**, *185*, 199−204.
(61) Finlay, J. A.; Bennett, S. M.; Brewer, L. H.; Sokolova, A.; Clay, G.; Gunari, N.; Meyer, A. E.; Walker, G. C.; Wendt, D. E.; Callow, M. E.; Callow, J. A.; Detty, M. R. Barnacle Settlement and the Adhesion of Protein and Diatom Microfouling to Xerogel Films with Varying Surface Energy and Water Wettability. *Biofouling* **2010**, *26*, 657−666.
(62) Sinde, E.; Carballo, J. Attachment of Salmonella Spp. and Listeria Monocytogenes to Stainless Steel, Rubber and Polytetrafluorethylene: The Influence of Free Energy and the Effect of Commercial Sanitizers. *Food Microbiol.* **2000**, *17*, 439−447.
(63) Melo, L. F.; Bott, T. R. Biofouling in Water Systems. *Exp. Therm. Fluid Sci.* **1997**, *14*, 375−381.
(64) Sun, Y.; Hoffman, A. S.; Gombotz, W. R. Non-Fouling Biomaterial Surfaces: II. Protein Adsorption on Radiation Grafted Polyethylene-Glycol Methacrylate Copolymers. *Polym. Prepr. (Am. Chem. Soc., Div. Polym. Chem.)* **1987**, *87*, 292−294.
(65) Zhao, C.; Li, L. Y.; Wang, Q. M.; Yu, Q. M.; Zheng, J. Effect of Film Thickness on the Antifouling Performance of Poly(Hydroxy-Functional Methacrylates) Grafted Surfaces. *Langmuir* **2011**, *27*, 4906−4913.
(66) Holmberg, K.; Quash, G. In *Biopolymers at Interfaces*, 2nd ed.; Malmsten, M., Ed.; Marcel Dekker: New York, 2003; pp 741−772.